Controlled in situ synthesis of Bi_2S_3/ZnS nano-film and its photoelectrochemical and photoresponsive performances

SHUANGSHUANG HU[a], WENLI QIN[a,b], SIQI JIA[a], PINGPING ZHANG[a,*], MANQING AI[a], SHIDI JIN[a], YING YE[a]
[a]*Departmen of Ocean Science,Ocean College, Zhejiang University, Zhoushan 316000, China*
[b]*College of Life and Environmental Science, Wenzhou University, Wenzhou 325035, China*

Novel Bi_2S_3 and Bi_2S_3/ZnS thin films have been synthesized through an in situ synthesis method at room temperature. Wide band gap ZnS and narrow band gap Bi_2S_3 composite to form heterojunction can show more excellent optoelectronic properties. The Bi_2S_3/ZnS thin films were then fabricated on FTO substrate, and this resulted in photocurrent to increase by 6 times compared to Bi_2S_3 thin films. Especially, response time and recovery time of the photodetectors was 0.04 s and 0.09 s, respectively. The photodetectors based on both semiconductor thin films show the features of linear photocurrent characteristics and good sensitivity.

(Received December 21, 2018; accepted June 14, 2019)

Keywords: Thin films, Bi_2S_3 – ZnS, Photoelectrochemistry, Photoresponse, In situ synthesis

1. Introduction

Bismuth sulfide (Bi_2S_3) plays an important role in thermoelectric devices, electronic and optoelectronic devices and infrared spectroscopy which has attracted considerable attention. In addition, Bi_2S_3 as an important semiconductor material has a reasonable band gap 1.3 - 1.7 eV [1] and it can be matched with photodiodes and photovoltaic cells. With the nanocrystallization of Bi_2S_3, it can not only cause blue shift of absorption wavelength and fluorescence emission, but also generate nonlinear optical response. Furthermore, it will also enhance the redox ability of nanoparticles and has superior photoelectrochemical and photocatalytic activity; in fact it shows broad application prospects in luminescent materials, nonlinear optical materials, and photocatalytic materials [2].

Various synthesis techniques of Bi_2S_3 nanomaterials have been reported in the literature; such as sonochemical method, high temperature method, microwave method, reflow method, template method [3], hydrothermal method (solvent heating) [4], vapor phase transfer method and ultrasonic method [5-7]. As the properties of nanomaterials are closely related to the morphology and size of the particles, the control of the synthesis of nanoparticles is a focus in the field of nanomaterial preparation, and is essential for film formation. By controlling the reaction conditions, it is possible to synthesize Bi_2S_3 with different morphologies. Currently, nanowires [8-10], nanorods [11, 12], nanosphere [13], nanotubes [14], nanoflowers [15], and nanoflakes [16] have been prepared. Though various Bi_2S_3 nanomaterials and their follow-up complex processing have been reported, few reports have focused on the preparation of Bi_2S_3 nano-film with nanosheet morphology.

The morphology of nano-Bi_2S_3 plays a decisive role in its photoelectrochemical properties. In order to obtain a controllable morphology of nanostructure via a simple and reliable route, it usually requires complicated, expensive, and high-energy consumption experimental instruments or reagents: these factors are not conducive to the expansion of production. It is still a huge challenge for industry to develop a low-cost method which can scale up production. On the other hand, compared with other semiconductor sulfides, Bi_2S_3 is a non-toxic and environmentally friendly photoelectric material, which is very beneficial for the control of environmental pollution [17].

Recently, as an important II - VI semiconductor with a wide band gap of 3.6 - 3.8 eV [18], ZnS has caused great interest in the field of optical coating material, photoconductors and photovoltaic devices as an ideal cadmium-free buffer layer material as it is environmentally friendly, resistant to high temperature deposition, and abundant in raw materials [19]. Heterojunctions of various sulfides have been prepared, such as Bi_2S_3/Bi_2O_3 [20], Bi_2S_3/Sb_2S_3 [21], ZnO/ZnS [22], Bi_2S_3/TiO_2 [23, 24]. Research on various grapheme [25-28] and its composite materials [29-31] is also very popular, Some heterostructured [32] graphene films such as graphene oxide composite films [33] and a free-standing superhydrophobic film [34], it Shows strong electrochemical performance [35] and energy conversion [36, 37].

However, there are still disadvantages such as

photo-etching, easily compounded photo-generated electron-holes, and absorption light range in the ultraviolet region. Compared with single-phase materials, the heterostructure formed by the combination of different functional components not only can exert the functional characteristics of different component materials, but also can receive better synergy, thus producing new features which differ from single-phase materials [38].

This in situ reaction process route has the following highlights: (1) the entire synthesis process was executed at room temperature with low energy consumption; an aqueous solution was used as a reaction system, no harmful or expensive reagent was used, and the synthesis product obtained was also non-toxic and environmentally friendly; (2) it has the advantages of simple and convenient operation, mild reaction conditions, short reaction cycle, and the uniform film can be prepared in large area; (3) ZnS grows in situ on the Bi_2S_3 nanofilm can evenly cover the surface of Bi_2S_3 to form a large number of heterojunctions. At the same time, it avoids a series of problems caused by the traditional film formation with powder material such as particle agglomeration, microstructure destruction, introduction of impurities, high temperature annealing, poor mechanical stability, etc.

In this work, the preparation and potential applications of Bi_2S_3-ZnS nano-film were reported through a template-free, room temperature and solution process route. The Bi_2S_3-ZnS nano-film was synthesised via a comparatively facile in situ reaction method.

2. Experimental sections

2.1. Materials

Zinc nitrate hexahydrate ($Zn(NO_3)_2{\cdot}6H_2O$), bismuth nitrate pentahydrate ($Bi(NO_3)_3{\cdot}5H_2O$), nitric acid (HNO_3), ammonia water ($NH3{\cdot}H_2O$), polyethylene glycol average Mn 6000 (PEG 6000, $HO(CH_2CH_2O)_nH$), sodium sulphate (Na_2SO_4, 99%), sodium borohydride ($NaBH_4$), ethanol (CH_3CH_2OH), triethanolamine ($(HOCH_2CH_2)_3N$) and ammonium sulfide ($(NH_4)_2S$) were purchased from Shanghai Aladdin Bio-Chem Technology Co., Ltd, China; all were of analytical grade and used as received without further purification. Distilled water was also used in all experiments.

2.2. Preparation of Bi_2S_3-ZnS nano-film

2.2.1. Preparation of Bismuth hydroxide

Bismuth hydroxide was synthesized via a reaction between bismuth nitrate hexahydrate and ammonia water using a hydrothermal process. Two mmol of bismuth nitrate pentahydrate was dissolved in 40 ml of 5 % nitric acid. While stirring, 13 ml of 5 % ammonia water was added, then add 0.01 g of polyethylene glycol. A white gelatinous substance appeared immediately, indicating the formation of $Bi(OH)_3$.

2.2.2. Preparation of Bi_2S_3-ZnS nano-film

$Bi(OH)_3$ was added into a suspension of a stoichiometric amount of $NaBH_4$ dissolved in 10ml ethanol under vigorous stirring, at the same time, adding a small amount of triethanolamine was useful for colloidal dispersion. A rapid color change was observed: the white colloidal solution became black which showed generation of bismuth. A small amount of nano-bismuth gel was placed in a beaker, sonicated for about 1 minute, then applied onto a clean FTO (15 Ω/sq) substrate to form a coating of about 1 cm square and allowed to stand for 12 hours to dry naturally at room temperature. After drying, the black nano-bismuth film was oxidized to a white bismuth oxide film. The FTO substrate was rapidly immersed in an ammonium sulfide solution (0.3 M) and removed immediately. The semi-dry film was immersed in deionized water for 20 s to remove soluble impurities. Finally, the above FTO substrates were immersed vertically in zinc nitrate hexahydrate solution (0.3 M) for 5 s, then immersed in an ammonium sulfide solution (0.3 M) for 5 s, washed and dried at room temperature. which (last two step) was repeated once, three times and six times denoted as BZ-1, BZ-2, BZ-3 respectively.

2.3. Characterization

The purity, and crystal structures of the obtained samples were confirmed using an X-ray diffractometer (XRD), and the XRD (XRD-6000, Shimadzu) patterns were recorded with a Curadiation of operation at 40 kV and 30 mA. The morphologies of prepared products were characterized by scanning electron microscopy (SEM, SU8010) which was equipped with EDS (X-MAX20, OXFORD). The optical property of samples were studied by UV-Vis absorption spectra which were recorded on a Shimadzu UV-2600 spectrophotometer.

2.4. Photoelectrochemical test

The PEC measurements were performed with an electrochemical analyzer (CHI760E, Chenhua Instruments, Shanghai, China) using a standard three-electrode, saturated Hg/HgCl/KCl and platinum electrode as the reference electrode and the counter electrode, respectively. The above samples were immersed in a 100ml quartz glass container with 0.5 M Na_2SO_4 solution which was used as the electrolyte to maintain the stability of the sulfide electrodes. A 500 W Xe arc lamp (QW500, Lansheng Instrument, Shanghai) served as the visible light source, and the lamp was illuminated for 20s continuously then shaded 20s as a cycle.

3. Results and discussion

Uniform Bi_2S_3 nanofilm and Bi_2S_3-ZnS nanofilm were synthesized via facile solution reaction process using Bi nanoparticles and Bi_2O_3 film as template. The morphology and size of products were examined by scanning electron microscopy (SEM). The high magnification SEM images (Fig. 1a) revealed that Bi nanoparticles were relatively rough and easy to condense, with a diameter ranging from 10 nm to 100 nm. Fig. 1b shows Bi_2O_3 films were relatively smooth except for a few slightly protruding films. As shown in Fig. 1c, a fairly smooth square can be seen, with side lengths ranging from 100 nm to 200 nm and thickness approximately is 15 nm. Morphology and uniformity are essential issues in the application of inorganic semiconductors. Their fairly regular array can increase the interface area and contribute to promote the transfer of electrons or holes between the interfaces. Figs. 1d-f show the SEM images of the Bi_2S_3-ZnS nanofilm with different immersion times, it can be seen that the addition of ZnS had strong effects on the formation of thinner nanofilm. In addition, a rough surface with large and small area of nanofilm can be clearly observed, also there are gaps between interfaces which can accelerate the transportation of electrons and holes. With an increased number of immersions, the thicknesses were decreased from 15 nm to 5 nm: the smaller the thickness, the wider the space.

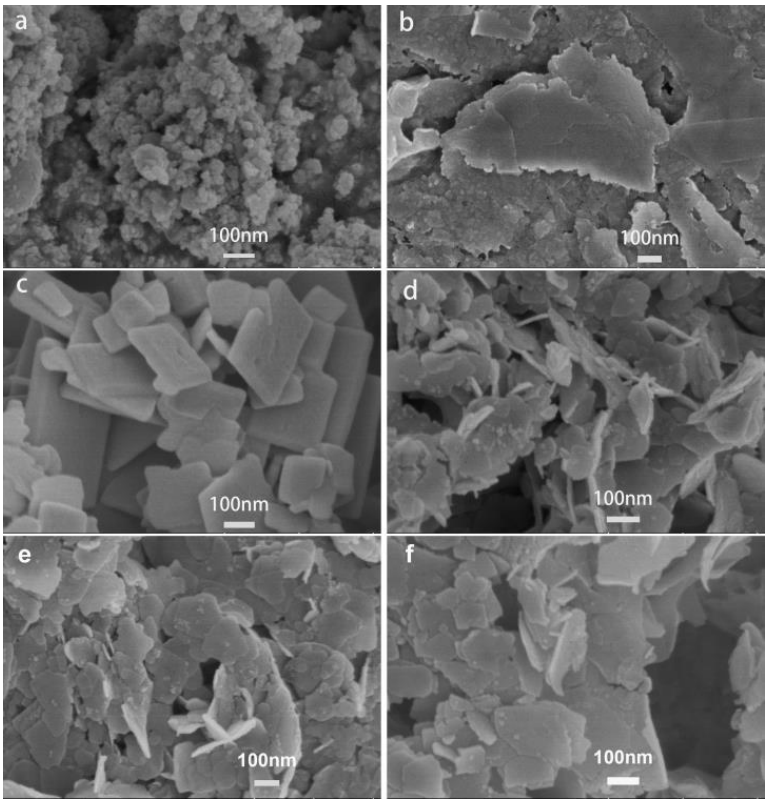

Fig. 1. SEM images of the Bi particle (a); Bi_2O_3 film (b); Bi_2S_3 film (c); BZ-1 (d); BZ-2 (e) and BZ-3 (f).

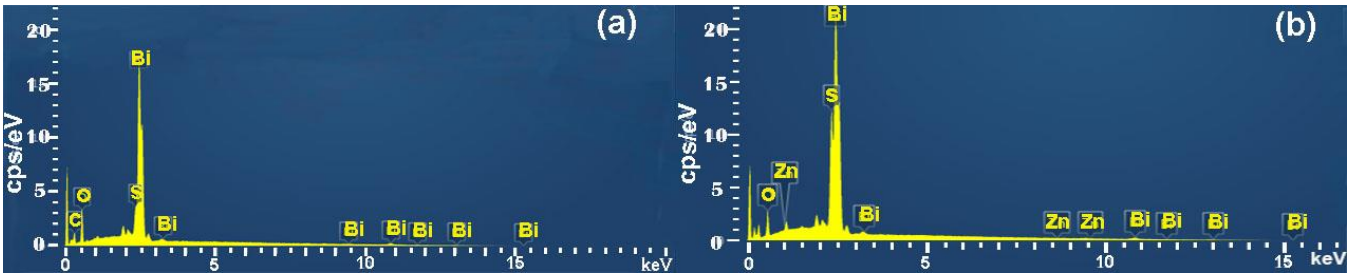

Fig. 2. EDS pattern of the (a) Bi_2S_3 film (b) and BZ-3.

The Bi_2S_3 film and BZ-3 samples were characterized using EDS analysis. Fig. 2a reveals the presence of elements of S, Bi, C and O, while the peaks of C and O were caused by the organic materials and background. Fig. 2b shows a typical EDS spectrum recorded on BZ-3, whose peaks are assigned to Zn, S, Bi, C and O, which

further confirmed the purity of the samples.

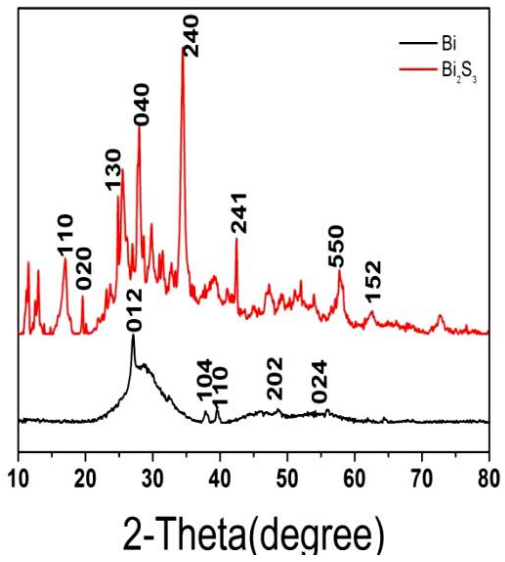

Fig. 3. XRD patterns of Bi and Bi_2S_3

Fig. 3 shows the patterns of Bi particles and Bi_2S_3 film. The diffraction peaks of Bi nanoparticles were indexed to trigonal (PDF # 44-1246) with lattice constants of a=4.547 Å, b=4.547 Å, and c=11.862 Å and the diffraction peaks with 2θ value around 27.17°, 37.95°, 39.62°, 48.68° and 25.04° could be observed, which could be indexed to (0 1 2), (1 0 4), (1 1 0), (2 0 2) and (0 2 4) plane, respectively. The result indicates they are pure phase. Relatively, the Bi_2S_3 after oxidation and surface sulfurization of Bi nanoparticles were exclusively indexed to orthorhombic (PDF # 17-0320) with lattice constants a=11.149 Å, b=11.304 Å, c=3.981 Å, which have stronger peaks of (1 1 0), (1 3 0), (0 4 0), (2 4 0) and weaker peaks of (0 2 0), (2 4 1), (5 5 0), (1 5 2). There are no characteristic peaks of any other phases detected in this pattern, so it proves very high purity of the samples.

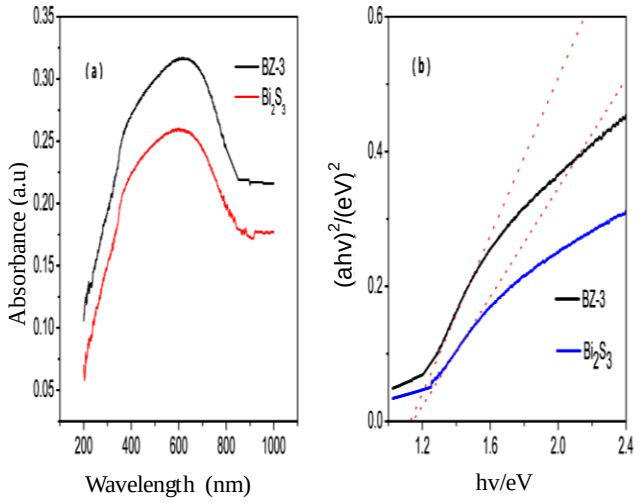

Fig. 4. (a) UV-Vis absorption spectra and (b) $(ahv)^2$ vs hv plots for the Bi_2S_3 and BZ-3

Fig. 4 (a) presents the optical absorption spectra of the Bi_2S_3 nanostructures and Bi_2S_3/ZnS composites. Both of the two samples clearly show an optical response in the visible region. They have strong absorption in the UV-Vis region of 200-800 nm, implying that the two samples may have photoelectrochemical performances. It also can be found that the Bi_2S_3/ZnS composites demonstrate more excellent optical absorption capability than Bi_2S_3 nanostructures.

The band gap energy of a semiconductor could be determined with the following formula:

$$(ahv)^2 = A(hv - Eg) \quad (1)$$

where a, h, v, A and Eg are the absorption coefficients, Plank constant, incident light frequency, characteristic constant, and band gap, respectively [39]. Therefore, the band gap energy (Eg value) of the resulting samples can be estimated from a plot of $(ahv)^2$ versus photon energy (hv). For semiconductors, the square of absorption coefficient is in linear relation with respect to energy for direct optical transitions in the absorption edge region, whereas the square root of absorption coefficient is linear with energy for indirect transitions. As shown in Fig. 4 (b), the intercept of the tangent to the X axis would give a good approximation of the band gap energy of the samples, which are corresponding to the band gaps of 1.16 eV and 1.18 eV, respectively, consistent with the previous reports. Furthermore, results suggest that the Bi_2S_3 is a direct semiconductor, in addition, the Bi_2S_3/ZnS composites do not show much difference from pure Bi_2S_3. However, the nanoscale heterostructures can be the active component in heterojunction solar cells due to their significant absorbance across the solar spectrum.

The on/off switching curve at the bias of 0.1V is shown in Fig. 5a. The Bi_2S_3-1 was the first test while the Bi_2S_3-2 was tested twenty minutes later. A low dark current of 0.5 μA and high photocurrent of -54 μA were measured in the first test, then decreased to a stable photocurrent of -22 μA. The photo response behavior of the Bi_2S_3 thin films could be expressed as follows [17]. In the dark, the oxygen molecules trapped at surface states form a low-conductivity depletion layer near the samples' surface: $O_2(g) + e^- \rightarrow O_2^-(ad)$; under the irradiation of light, the samples would generate electron-hole pairs and then separate in the Bi_2S_3 thin films, at this time, the negative oxygen ions released their own electrons to the generated holes, forming a recombination of surface electron-holes. $h^+ + O_2^-(ad) \rightarrow O_2(g)$. Unpaired electrons accumulated and increased photocurrent formed a distinct photocurrent density peak (J_{in}). The measured photo response current increased continuously, J_{in} decreased in a decelerated fashion until equilibrium was attained. This phenomenon may be attributed to inevitable e^-/h^+ recombination.

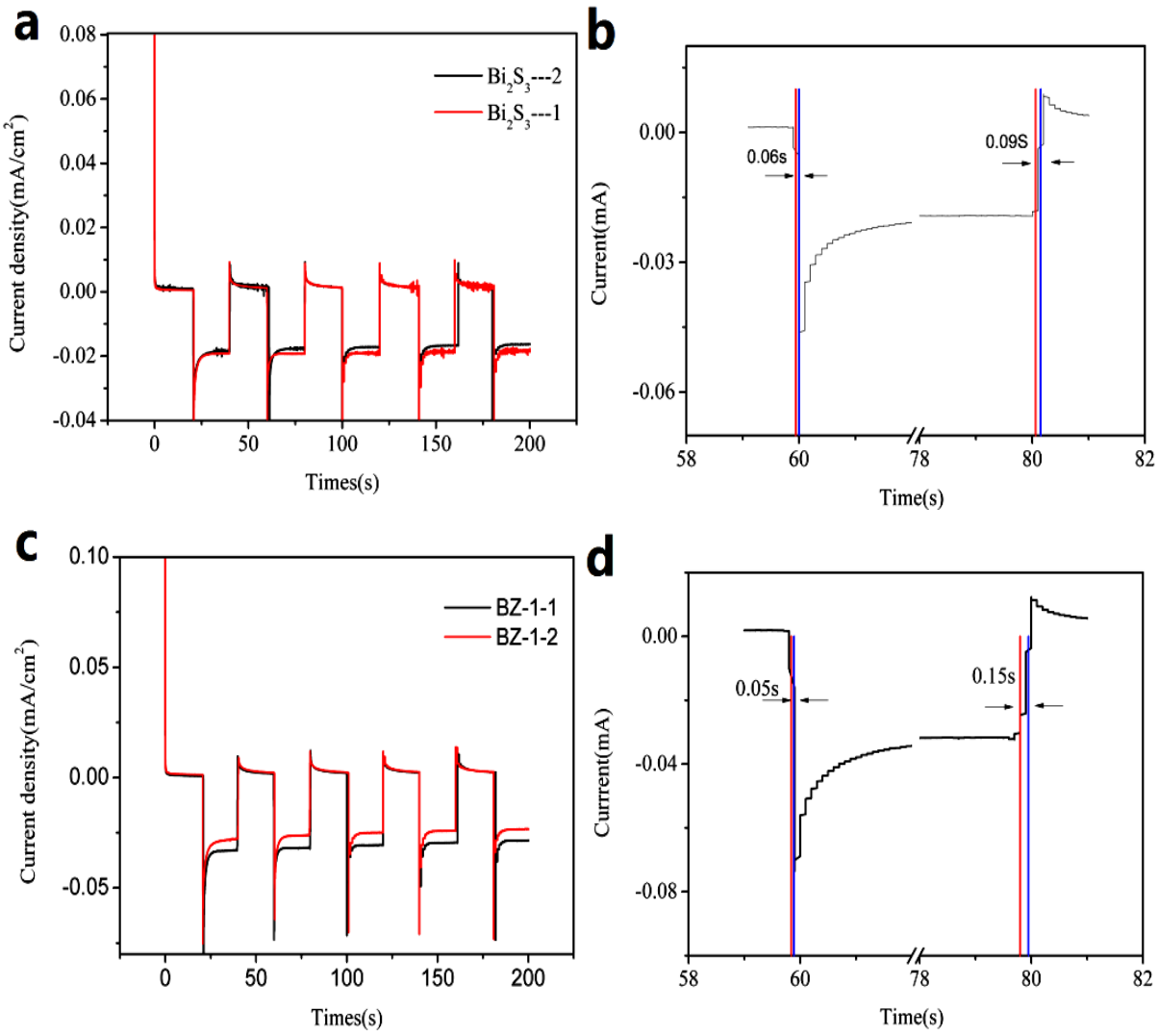

Fig. 5. (a) Photoresponsive curves of FTO/Bi_2S_3 devices at 0.1 V bias, (b) enlarged view of a single on/off cycle of the FTO/Bi_2S_3-1 devices, (c) Photoresponsive curves of FTO/Bi_2S_3 /ZnS-1-1 devices at 0.1 V bias, (d) enlarged view of a single on/off cycle of the FTO/Bi_2S_3/ZnS devices

Electrons are likely to recombine with holes during the transfer process, resulting in the decay of J_{in}. Once the production rate and the recombination rate reached equilibrium, the steady state photocurrent density (J_{st}) was achieved. When the light was off, the electron-hole pairs were quickly recombined, however, there was still a lot of electronics left on the surface, eventually reoccupied by oxygen molecules, causing the J_{st} to drop rapidly. Once the irradiation was turned on again, J_{in} returned to the original value. The J_{in} and J_{st} values remained closely constant in on-off cycles. Compared with Bi_2S_3-1, the stable photocurrent was reduced a little to -20 μA. As time went by, from the curves, we found that there was a slight decrease in the photocurrent of the device after twenty minutes, indicating a great stability of the device.

PEC applications of photoresponsive semiconductor nanomaterials are attracting people's attention, meanwhile there are several applications worth studying such as optical switches and photodetectors, which play an important role in imaging techniques, optoelectronic circuits, and light communications. As for high-performance photodetectors, the response capability of the photoactive materials is the staple element, because a slow time response acquired will become a limitation of the material application. Fig. 5b shows the enlarged views of a single on/off cycle of the FTO/Bi_2S_3 device. The response time is defined as the 10% and 90% points of the maximum photocurrent, and the recovery time is defined from the 90% point to the 10% point of the maximum photocurrent [26]. As can be seen from Fig. 5b, the device's response time and recovery time were measured to be 0.06 s (59.94 s-60 s) and 0.09 s (80.06 s-80.15 s), separately. As is well known, the response of a material to the illumination of light with different wavelengths is mainly decided by their band gap. Different band gap semiconductors combined can exceedingly enhance the

visible light capture capability. Therefore, the ZnS was applied on the Bi_2S_3 for once only (see Fig. 5c). Compared with the Bi_2S_3-1 under the same condition, the stable photocurrent density was measured to 36 μA, increased about 1.6 times. Different band gap materials can absorb different wavelengths of visible light, so its addition facilitates the absorption of shorter wavelength light. However, the stability of the flexible device was slightly reduced after twenty minutes. As for the response and recovery time, they were nearly identical and had the same response rate.

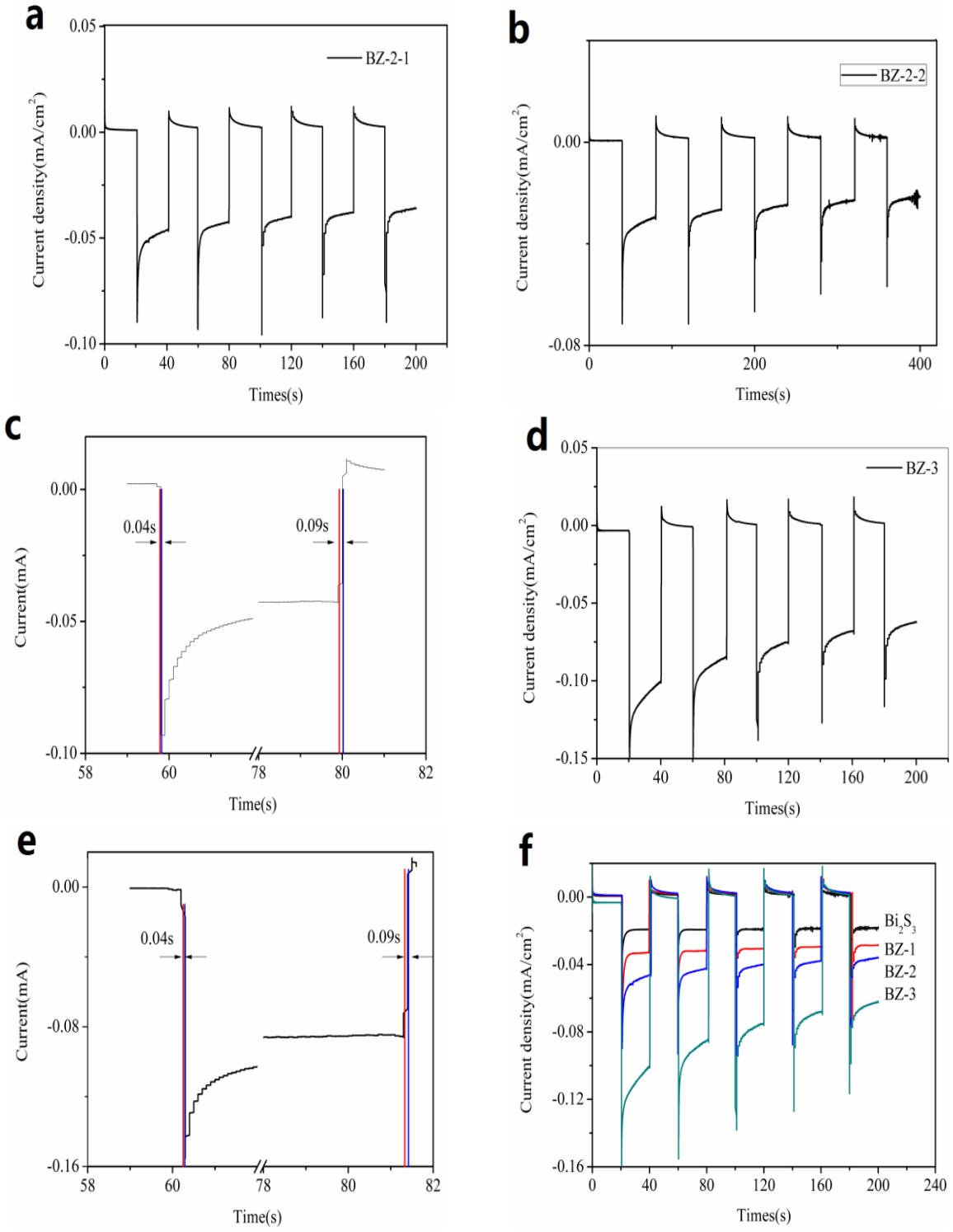

Fig. 6. (a) Photoresponsive curves of FTO/Bi_2S_3/ZnS-2-1 devices at 0.1 V bias, (b) Photoresponsive curves of FTO/Bi_2S_3/ZnS-2-2 devices at 0.1 V bias which was measured twenty minutes later with additional on/off cycles, (c) enlarged view of a single on/off cycle of the FTO/Bi_2S_3/ZnS-2-1 devices, (d) Photoresponsive curves of FTO/Bi_2S_3/ZnS-3 devices at 0.1 V bias, (e) enlarged view of a single on/off cycle of the FTO/Bi_2S_3/ZnS-3 devices, (f) Photoresponsive curves of all devices

Fig. 6a shows the photoresponse of the FTO/Bi_2S_3 /ZnS-2-1 devices as a function of time under a small bias of 0.1 V. On the original basis, coated with two layers of ZnS, the device gave reproducible photocurrent responses with stable photocurrent density which was measured to 60 μA to the regular chopped illumination. The on/off sensing cycles could be repeated over a long period of time without apparent deterioration. The response and recovery time of the device were gauged to be 0.04 s (59.78 s-59.82 s) and 0.09 s (79.93 s-80.02 s). Furthermore, compared with the previous two samples, this photodetector displayed a superior switching ratio, the photocurrent density was increased to a stable value (60 μA), the value was almost three times as much as pure Bi_2S_3, demonstrating the advantage of the Bi_2S_3 /ZnS. Based on this photodetector, three additional layers of zinc sulfide were added. Fig. 6d shows that the photocurrent of the FTO/Bi_2S_3 /ZnS-3 exhibited a significant increase under sunlight illumination, which was further proved by the time-dependent photoresponse of the device (see Fig. 6e). The photocurrent density was increased to a value (120 μA); the value was almost six times as much as pure Bi_2S_3, demonstrating the advantage of the Bi_2S_3/ZnS once again. However, the photocurrent density value in order to achieve equilibrium, declined to 70 μA eventually after constant on/off cycles, but the response and recovery time of the device had no major changes. Fig. 6f includes whole photoresponsive curves of photodetector devices. First of all, the photocurrent density increased while coated with a layer of ZnS because the surface area became larger for thicker films of Bi_2S_3 /ZnS-1, resulting in more electrons to be captured with a larger surface area. However, after five layers of ZnS were added, the initial photocurrent density became larger, but the attenuation increased and the instability became higher. This is because an over-thick film of Bi_2S_3/ZnS leads to a long transportation path for carriers, therefore, electrons and holes are highly likely to recombine. As described above, in order to ensure the photocurrent and stability, a suitable film coating time is required for efficient production and separation of electron-hole pairs. A thinner coating film had a lower generation efficiency of electron-hole pairs due to less absorption of light, and a thicker coating film had a low separation ability of electron-hole pairs due to their recombination during the long transportation path of carriers.

4. Conclusions

In summary, Bi_2S_3 nano-film and Bi_2S_3/ZnS nano-film have been successfully prepared using an efficient in situ synthesis process at room temperature. By taking advantage of a pre-coated nano Bi layer on the FTO glass, which provides a more simple, environmental-friendly, convenient and economic means of mass producing Bi_2S_3 nano-film and Bi_2S_3/ZnS nano-film which is based on Bi_2S_3 nano-film. The enhanced activities of Bi_2S_3/ZnS nano-film can be attributed to the effective separation and generation of carriers. The information offered here is expected to be useful for the synthesis of other sulfide materials' combination to acquire better photoelectrochemical capacity. Therefore, this production route may be economical for a scale up process, a photodetector modified by the as-prepared Bi_2S_3/ZnS nano-film exhibited enhanced photoelectrochemical activty, which are promising for potential applications in PEC devices such as photoelectrochemical cells and photoelectronic switches. Moreover, the photoelectrochemical (PEC) devices exhibited photosensitivity with the features of rapid response and recovery time, high on/off ratio and stable switching cycle performance. In addition, it may guide the fabrication of naval photoactive materials for photovoltaic industry.

Acknowledgements

We are grateful for the technical support of Dr. Ying Ye. The authors are thankful to Siqi Jia for help with the experiments. This study was supported by the Study on Oil and Gas Resource Potential of Tarim Marine Carbonate Project (529000-RE1201).

References

[1] S. A. Patil, Y. Hwang, V. V. Jadhav, K. H. Kim, H. Kim, J. Photoch. Photobio. A **332**, 174 (2017).
[2] Y. F. Lu, M. F. Ye, C. Y. Wei, L. X. Xu, G. C. Chen, T. F. Yi, New Chem. Mater. **43**(4), 6 (2015).
[3] J. R. Ota, S. K. Srivastava, Nanotechnology **16**(10), 2415 (2005).
[4] H. Zhang, D. Yang, S. Li, Y. Ji, X. Ma, D. Que, Nanotechnology **15**(9), 1122 (2004).
[5] H. Yin, Wuhan University of Technology **09**, 46 (2009).
[6] Z. K. Zhu Qi'An, China Sci and Technology Core Journal **03**, 58 (2013).
[7] J. W. Fang Qin, Journal of Beijing University of Science and Technology **05**, 638 (2010).
[8] M. Z. A. H. Zhisong Lu, Nanotechnology **15**, 1122 (2017).
[9] G. Kunakova, J. Katkevics, A. Viksna, Z. Gertnere, J. Varghese, J. D. Holmes, Electrochim. Acta **170**, 33 (2015).
[10] R. Li, Q. Yue, Z. Wei, J. Mater. Chem. C **1**, 5866 (2013).
[11] X. Zhou, X. Zhao, D. Zhang, S. Chen, X. Guo, W. Ding, Y. Chen, Nanotechnology **17**, 3806 (2006).
[12] Y. Wang, J. Chen, P. Wang, L. Chen, Y. Chen, L. Wu, The Journal of Physical Chem. C **113**(36), 16009 (2009).
[13] L. Ma, J. Wu, S. Wang, H. Yang, D. Liang, Z. Lu, J.

Inorg. Biochem. **168**, 38 (2017).
[14] S. Kumar, S. Sharma, S. Sood, A. Umar, S. K. Kansal, Ceram. Int. **42**, 17551 (2016).
[15] F. Cao, J. Wang, W. Tu, X. Lv, S. Li, G Qin, Mater. Res. Bull. **68**, 115 (2015).
[16] J. Chao, S. Xing, Y. Zhao, S. Gao, Q. Song, L. Guo, D. Wang, T. Zhang, Solid State Sci. **61**, 51 (2016).
[17] S. A. Patil, Y. Hwang, V. V. Jadhav, K. H. Kim, H. Kim, J. Photoch. Photobio. A **332**, 174 (2017).
[18] P. Chen, L. Gu, X. Cao, Crystengcomm. **12**, 3950 (2010).
[19] K. Qiu, D. Qiu, L. Cai, S. Li, W. Wu, Z. Liang, H. Shen, Mater. Lett. **198**, 23 (2017).
[20] F. Liu, Y. Yang, J. Liu, W. Huang, Z. Li J, Electroanal. Chem. **665**, 58 (2012).
[21] Y. Huang, G. Xie, S. Chen, S. Gao, J. Sold. State Chem. **184**, 502 (2011).
[22] P. Chen, L. Gu, X. Cao, Crystengcomm. **12**, 3950 (2010).
[23] S. Kumar, S. Sharma, S. Sood, A. Umar, S. K. Kansal, Ceram. Int. **42**, 17551 (2016).
[24] J. H. H. Z. Haijing, Nanotechnology **25**, 2157020 (2014).
[25] J. Pang, R. G. Mendes, P. S. Wrobel, M. D. Wlodarski, H. Q. Ta, L. Zhao, L. Giebeler, B. Trzebicka, T. Gemming, L. Fu, Z. Liu, J. Eckert, A. Bachmatiuk, M. H. Rümmeli, ACS Nano **11**, 1946 (2017).
[26] K. Olszowska, J. Pang, P. S. Wrobel, L. Zhao, H. Q. Ta, Z. Liu, B. Trzebicka, A. Bachmatiuk, M. H. Rummeli, Synthetic Metals **234**, 53 (2017).
[27] K. Wang, L. Li, Y. Lan, P. Dong, G Xia, Math. Probl. Eng. **201**, 1 (2019).
[28] Q. Hao, J. Pang, Y. Zhang, J. Wang, L. Ma, O. G Schmidt, Adv. Opt. Mater. **6**, 1700984 (2018).
[29] L. L. X. W. Wang Kai, Int. J. Electrochem. Sci. **12**, 8306 (2017).
[30] Y. Lei, F. Chen, R. Li, J. Xu, Appl. Surf. Sci. **308**, 206 (2014).
[31] C. F. X. B. Zheng Zhang, Materials **11**, 512 (2018).
[32] R. G Mendes, J. Pang, A. Bachmatiuk, H. Q. Ta, L. Zhao, T. Gemming, L. Fu, Z. Liu, M. H. Rümmeli, ACS Nano **13**, 978 (2019).
[33] K. Wang, J. Pang, L. Li, Front. Chem. Sci. **12**, 376 (2018).
[34] F. Shu, M. Wang, J. Pang, et al, Front. Chem. Sci. **23**, 2095 (2018).
[35] Z. S. Z. Y. Wang Kai, Int. J. Electrochem. Sci. **13**, 10766 (2018).
[36] R. G M. Jinbo Pang, Chem. Soc. Rev. **48**, 72 (2019).
[37] J. Pang, A. Bachmatiuk, Y. Yin, B. Trzebicka, L. Zhao, L. Fu, R. G Mendes, T. Gemming, Z. Liu, M. H. Rummeli, Adv. Energy Mater. **8**, 1702093 (2018).
[38] X. Y. Xu, Nanjing University of Science and Technology **02**, 67 (2016).
[39] J. Chao, S. Xing, Y. Zhao, S. Gao, Q. Song, L. Guo, D. Wang, T. Zhang, Solid State Sci. **61**, 51 (2016).

*Corresponding author: marin011@zju.edu.cn